A COORDINATED DOCKING APPROACH BASED ON EMBEDDED VISION

Zhao Peng,* Cao Zhiqiang,* Gu Nong,** Zhou Chao,* Xu De,* and Tan Min*

Abstract

Docking is an essential yet challenging problem to the deployment of marsupial robotic system involving a mother robot and several child robots, as the technologies such as rail-line tracking and global vision measurement are not suitable for applications in unknown environments. This chapter presents a coordinated docking approach based on embedded vision of the child robot collaborated by the mother robot with an innovative lifting docking station. The child robot utilizes a complementary metal oxide semiconductor (CMOS) camera to capture and extract image features related to a benchmark attached on the docking station, and the internal correlation between its heading direction and the entry direction of docking station is then derived, which makes the docking process be concise and convenient. On this basis, a coordinated docking task model is built and the transition conditions among task states are presented. The precision analysis of the docking is also discussed. The experimental results prove the effectiveness of the proposed approach.

Key Words

Marsupial robotic system, coordinated docking, embedded vision, lifting docking station

1. Introduction

Multi-robot system has been attracting more and more attentions with advantages such as parallelism and robustness [1]. Existing researches have focused on the problems of tasks and resource distribution, conflict resolution, cooperative planning, swarm intelligence, *etc* [2]–[6]. With the expansion of applications, it is noted that some practical tasks involving environmental detection, mine exploration or survival search and rescue often require the robots to entrance many narrow spaces, which means the size of robots shall be reduced with on-board battery and computing ability. As a result, the long-distance travel for these robots becomes fatal. How to adapt narrow environments for a multi-robot system with powerful voyage ability becomes a challenging issue.

* Institute of Automation, Chinese Academy of Sciences, Beijing 100190, China; email: {peng.zhao, zhiqiang.cao, chao.zhou, de.xu, min.tan}@ia.ac.cn

** Centre for Intelligent Systems Research, Deakin University, Waurn Ponds, VIC, Australia; email: nong.gu@deakin.edu.au
Corresponding Author: Cao Zhiqiang

Inspired by nature, marsupial animals like kangaroos, Murphy *et al.* offered an innovative solution named marsupial robotic society [7]. A typical marsupial robotic team consists of a transporting mother robot and several size-limited but power-restricted child robots. With smaller sizes and special skills, child robots adapt to specific environments or tasks that are beyond scopes and abilities of the mother robot. With the assistance of localization, signal relay, power recharge and especially the long-distance transportation from the mother robot, the child robots can overcome defects caused by the shortage of resources. In marsupial robotic systems, an individual member may have different types: unmanned ground vehicle (UGV), unmanned surface vehicle (USV), unmanned aerial vehicle (UAV) or autonomous underwater vehicle (AUV). At present, the developed categories of marsupial robotic systems [8]–[12] include UGV-UGV system, USV-UAV alliance, UGV-UAV cooperation and AUV-AUV combination. As one of the most widely used type, UGV-UGV marsupial system receives more attentions, especially in the field of urban exploration and rescue. The marsupial robotic system with the Mobile Automated Characterization System (MACS) and Reduced Access Characterization Subsystem (RACS) was designed to characterize intense levels of indoor radiation [13]. MACS is a large mobile automated system, and it utilizes multi-radiation detectors to characterize spacious rooms, while RACS takes effect in narrow floor space that is inaccessible to MACS. Dellaert *et al.* used a wheeled mobile robot to carry four-legged Aibo robots for survival rescue [14]. The wheeled mobile robot serves as the role of mother to provide computation and sensor resources to map scenes after a disaster, and each Aibo robot is transported to explore suspicious locations of survivors with an on-board camera capturing images and transmitting them to the console. The Silver Bullet–Bujold team presented another practical marsupial robotic system where the mother robot Silver Bullet provides power and on-board computation resource, and the child robot Bujold changes its shape to adapt to the environment for capturing information with the on-board camera and microphone [15]. A similar system was exploited for application in rescue concerning mine disasters [16]. Papanikolopoulos and coworkers have been dedicated to the marsupial robotics for years with contributions on design of miniature robots, docking station, longevity optimization and power management [17]–[20].

Docking is especially important for marsupial robots, which requires accurate control on both relative position and orientation between the child robot and its mother robot. Because the child robots usually work in unknown environments with limited sensors/computation resource, the traditional pose sensing and servoing technologies are not suitable for them, such as navigation reckoning with a priori maps, global vision measurement *via* a fixed overhead camera or rail-line patrol relying on magnetic and photoelectric detectors. Fortunately, vision-based docking with an on-board camera offers a better option. In [21] and [22], visual benchmarks were mounted on the docking station. The child robots capture the images *via* the on-board cameras and transmit them to a PC for image processing whose results are returned to the child robots for decision making. A robust vision algorithm using adaptation and imprinting for docking was proposed in [23], which ran on the mother robot. In [2] and [24], a camera was mounted on the top of docking station to direct the child robot docking into it.

The docking based on wired image transmission shall limit the activity range of the child robot. This problem can be resolved by transmitting images wirelessly to the mother robot. However, it shall be unstable considering the limited wireless bandwidth and unexpected disturbance. The method based on visual observation of the mother robot does not require image transmission. Unfortunately, the visual field is limited due to the smaller size of the child robot and downward pose of camera fixed on the station, which leads to a reduced effective docking zone. In order to deal with these problems, the autonomous docking based on embedded vision of child robot becomes promising. In addition, very few reports on docking involving the motion of the mother robot have been given, although the participation of the mother robot shall simplify the alignment difficulty of relative pose and reduce the task execution time.

The contribution of this chapter is as follows. It presents an embedded vision-based docking approach that involves the motion of the mother robot for fast docking. Specifically, according to the extracted features of the benchmark, the internal correlation between the entry direction of docking station and the heading of child robot are derived, which makes the docking process become concise and convenient to be applied.

The remainder of this chapter is organized as follows. Section 2 formulates the problem to be investigated. The docking approach including the internal correlation between the entry direction of docking station and the heading of child robot is given in detail in Section 3. Section 4 demonstrates the experimental results and Section 5 concludes the chapter.

2. Problem Statement

The results of this chapter are motivated by the problem of coordinated docking for the marsupial robotic system, where the child robot is required to enter the docking station autonomously and quickly based on embedded vision with the coordination of the mother robot. As shown in Fig. 1, a docking station with a lifting platform is mounted at the rear of the mother robot and a benchmark formed by four equal rectangle blocks with two colours is hanged on the lifting platform. Clearly, there are two crossing line segments corresponding to colour border, and the horizontal one is labelled as H_{GS} with its midpoint labelled as I_h. A camera is fixed on the child robot, inclined upward with an angle $\theta(\theta \in (0, \pi/2))$.

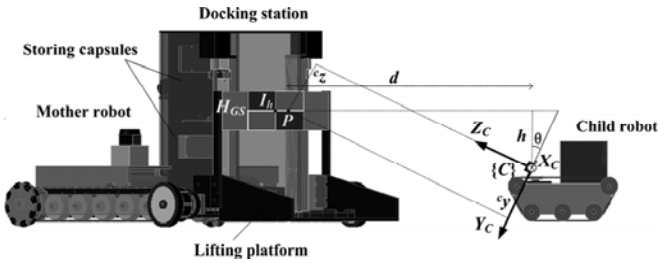

Figure 1. The coordinated docking based on embedded vision.

We establish the camera coordinate frame $\{C\}$ with its Z_C axis being the optic axis of the camera. Taking an arbitrary point P in H_{GS}, the coordinate $({}^cy, {}^cz)$ of point P in the Y_CZ_C plane of $\{C\}$ can be calculated as follows:

$$\begin{cases} {}^cy = (d + h\tan\theta)\sin\theta - h\sec\theta \\ {}^cz = (d + h\tan\theta)\cos\theta \end{cases} \tag{1}$$

where $h(h > 0)$ is the altitude difference between H_{GS} and the camera and d is the lateral distance between the point P and the camera. Besides, we also build a ground frame $\{R\}$ for the child robot, as shown in Fig. 2. Its origin O_R is the projection point of the camera on the ground, and Y_R axis is coincident with its heading direction. H'_{GS} is the projection of H_{GS} in $\{R\}$, and its normal vector is described with $\overrightarrow{VE}(\cos\alpha, \sin\alpha)$ where $\alpha(\alpha \in (0, \pi))$ is the entry angle of the docking station. The projection point of I_h in $\{R\}$ is labelled as $E(x_e, y_e)$. When the line segment H_{GS} is captured by the camera, the angle between the vector $\overrightarrow{VE}$ and the position vector $\overrightarrow{O_RE}$ shall be an acute one, then we have formula (2):

$$\overrightarrow{O_RE} \cdot \overrightarrow{VE} = x_e\cos\alpha + y_e\sin\alpha > 0 \tag{2}$$

From Fig. 2, the x-coordinate ${}^cx$ of point P in $\{C\}$ is equal to that of point P' in $\{R\}$, where P' is the projection of P in $\{R\}$. Then, we have

$${}^cx = x_e - (d - y_e)\tan\alpha \tag{3}$$

Therefore, the image coordinates (u_p, v_p) of an arbitrary point P in H_{GS} in $\{C\}$ is obtained as follows:

$$\begin{bmatrix} u_p \\ v_p \end{bmatrix} = \begin{bmatrix} k_x & 0 & u_0 \\ 0 & k_y & v_0 \end{bmatrix} \begin{bmatrix} {}^cx/{}^cz \\ {}^cy/{}^cz \\ 1 \end{bmatrix} \tag{4}$$

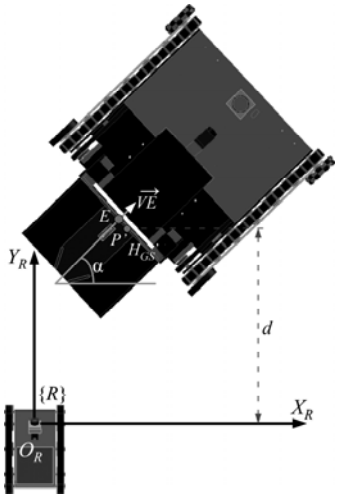

Figure 2. The projection of horizontal colours borderline segment H_{GS} in $\{R\}$.

where k_x and k_y are the scale factors of u and v axes in the image plane, and (u_0, v_0) are the coordinates of the principal point in the image plane.

The child robot extracts the image features of the benchmark. The horizontal coordinate u_h of I_h, the imaging slope k_h of H_{GS} in the image plane, and the horizontal coordinate length s_u of H_{GS} are utilized to direct the motion of the child robot. These features instead of image/video data are transmitted to the mother robot for an effective coordination.

With the definitions and symbols mentioned above, the objective of this chapter is stated as follows.

Given a UGV-UGV marsupial robotic system whose child robot is assembled with an on-board camera, find a coordinated scheme that steers the child robot and the mother robot based on the extracted image features (u_h, k_h, s_u) such that the system achieves a fast docking without the calibration of the camera.

3. The Coordinated Docking Approach

3.1 Image Features Extraction

This chapter considers the benchmark with red and green coloured rectangle blocks (see Fig. 1). The image features are extracted based on loose colour attributes and arrangement of these blocks. The first step is to search the pixel points possibly surrounding I_h, and it starts from the upper left pixel. According to the colour attributes around I_h, for the pixel point (i, j) whose main component is red, we shall check whether the main components of pixel points $(i, j+8)$, $(i+8, j+8)$ and $(I+8, j)$ are green, red and green, respectively. The pixel points passing all checks are combined into either the nearest candidate group or a new group. After the traverse process is finished, the candidate group with maximum number N_G of pixel points is chosen with the premise of $N_G \geq T_N$, where T_N is a given threshold. The coordinates values of all pixel points in the chosen group are averaged as that of $I_h(u_h, v_h)$.

Figure 3. An illustration of image features extraction, where $u_h = 293$, $S_u = 39$ and $k_h = -0.0762$.

Next, lateral red/green border pixel points are searched to extract k_h. Take the left search as an example. A pixel point (u_i, v_i) is regarded as a lateral border point if the main component of $(u_i, v_i - 2)$ and $(u_i, v_i + 2)$ are red and green, respectively. With all lateral border points, s_u is acquired and the least square fitting method is utilized to calculate the imaging slope k_h as follows:

$$k_h = \frac{\sum_{i=1}^{S_u} (u_i - \overline{u})(v_i - \overline{v})}{\sum_{i=1}^{S_u} (u_i - \overline{u})^2} \tag{5}$$

where $\overline{u}$ and $\overline{v}$ are the mean values of u_i and v_i, respectively.

Figure 3 gives an illustration for a real image captured by the CMOS camera of the child robot, where the chosen candidate group is labelled in black circle with $N_G = 120$, and the horizontal border H_{GS} is extracted and outlined.

3.2 Implications of Image Features for Docking

When the child robot points at the docking station, u_h is close to the vertical bisector of the image and s_u increases as the docking distance decreases. In order to achieve autonomous docking for the child robot, the analysis of internal correlation between its heading direction and the entry direction of docking station is very meaningful. Let us take two arbitrary points A and B in H_{GS}, and the theoretical imaging slope $\overline{k_h}$ of k_h is derived with formulas (1), (3) and (4):

$$\overline{k_h} = \frac{v_A - v_B}{u_A - u_B} = \frac{-k_y h \cos\alpha}{k_x(x_e \cos\alpha + y_e \sin\alpha + h \tan\theta \sin\alpha)\cos\theta} \tag{6}$$

Under the constraints described by formula (2) with $\theta \in (0, \pi/2)$ and $h > 0$, the denominator of formula (6) is always positive, which means that the algebraic sign of $\overline{k_h}$ depends on $\overrightarrow{VE}(\cos\alpha, \sin\alpha)$. Therefore, we have

Remark 1: *When the vector* $\overrightarrow{VE}(\cos\alpha, \sin\alpha)$ *is in accordance with the heading of child robot,* $\alpha = \pi/2$. *From formula (6), the value of* $\overline{k_h}$ *is 0, which implies that the imaging line segment of* H_{GS} *is horizontal in*

the image plane. $\overline{k_h}$ *is negative when* $\alpha < \pi/2$ *and vice versa.*

Remark 2: *When the camera points at the entrance of docking station, the absolute value* $|\overline{k_h}|$ *is positively correlated with the angular offset* $|\pi/2 - \alpha|$ *and negatively correlated with the distance between the child robot and its mother robot. Furthermore, if the image features* k_h *and* s_u *meet the constraint set* $\{|k_h| \geq \left|{}^i k_h\right| \cap s_u \geq {}^i s_u | ({}^i k_h, {}^i s_u) \in f_{list}, i = 1, 2, ...\}$, *where* f_{list} *is a list of recorded image features when the child robot is put at different positions with a criterion distance around the benchmark, it can be confirmed that the distance from the child robot to docking station is no more than this criterion distance.*

Remark 3: *Before the child robot moves straight directly to board the lifting platform of docking station, it is required to move closely to the entrance and match its heading with the entrance direction of the docking station, that is*

$$\begin{cases} k_h \in (-\Delta k, \Delta k) \\ \mathrm{u_h} \in \left(W/2 - \Delta u, W/2 + \Delta u \right) \\ \mathrm{s}_u \geq s_u^e \end{cases} \tag{7}$$

where W *is the width of the image,* Δu *and* Δk *are tolerance margins of* u_h *and* k_h, *respectively,* s_u^e *is a pre-measured image feature criterion of* s_u *under a visual perception criterion distance* d_e *along the entry direction of docking station.*

3.3 Coordinated Docking

In the following, a coordinated scheme involving the child robot and its mother robot is presented with the utilization of image features (u_h, k_h, s_u). As shown in Fig. 4, the docking process is described as follows. First, the child robot rotates on the spot, so does the mother robot but with a slower angular speed to make sure the benchmark to be captured by the child robot. Later, the child robot approaches the docking station with the guide of image feature u_h until it reaches to the surrounding area of the station according to **Remark 2**. In the same time, the mother robot rotates to align the station pose with **Remark 1**. After that, the mother robot still rotates on the spot slowly, and the child robot advances and rotates alternately until the formula (7) in **Remark 3** is met (see Fig. 4(c)). It is noted that if the child robot cannot extract the image features in a few successive frames, it shall rotate on the spot to capture the benchmark again. Finally, the child robot moves straight and boards the lifting platform of docking station. This platform shall elevate the child robot to its expected storing capsule, as shown in Fig. 4(d). As stated above, the child robot has four task states including *linking*, *approaching*, *matching*, and *directed* states, and the mother robot possesses three task states, such as *linking*, *aligning*, and *directing states*, as shown in Fig. 5.

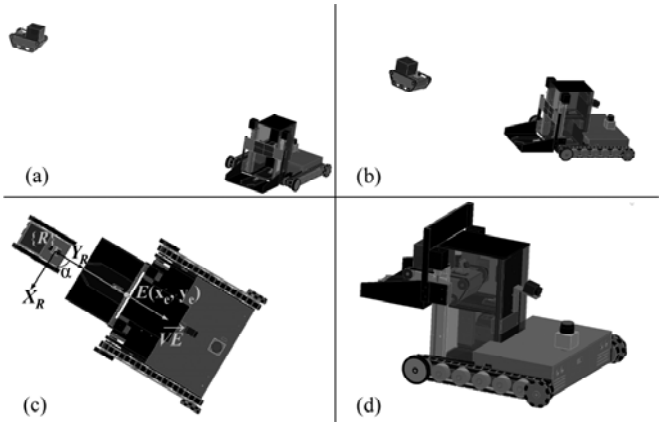

Figure 4. Coordinated docking between the child robot and mother robot.

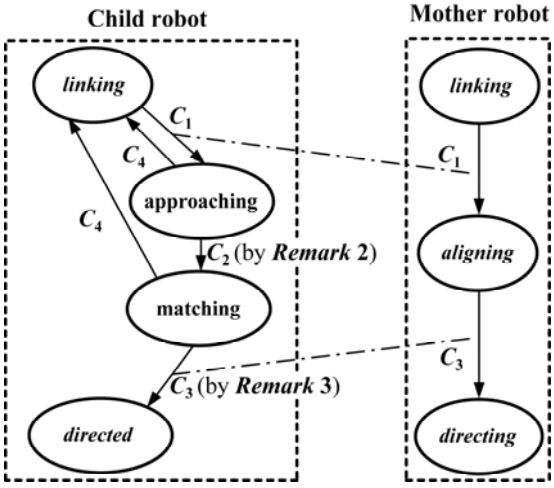

Figure 5. Task model of the coordinated docking.

The transition conditions $C_1 \sim C_4$ are given by referring to the ***Remarks*** in Section 3.2, where C_1 shows that the benchmark is captured; C_2 shows that the child robot approaches the station with a certain range around the docking station (see ***Remark* 2**); C_3 shows that the image features satisfy the restrictions by ***Remark* 3**; C_4 shows that the image features have been lost for a few successive frames. The flow chart of the docking is given in Fig. 6.

3.4 Precision Analysis

A successful docking depends on the width deviation Δx_e and entry direction offset $\Delta\alpha$ in the final docking stage, as illustrated in Fig. 7, where the coordinate of projection point of I_h in $\{R\}$ is $E(\Delta x_e, d_e)$, and $\Delta\varepsilon$ is the angle between Y_R-axis and $\overrightarrow{O_R E}$; b_e and b_c are the width of entrance of the docking station and the width of the child robot, respectively.

From Fig. 7, it is seen that a successful docking should satisfy the following formula:

$$\frac{b_e \cos|\Delta\alpha|}{2} > |\Delta x_e| + \frac{b_c}{2} \tag{8}$$

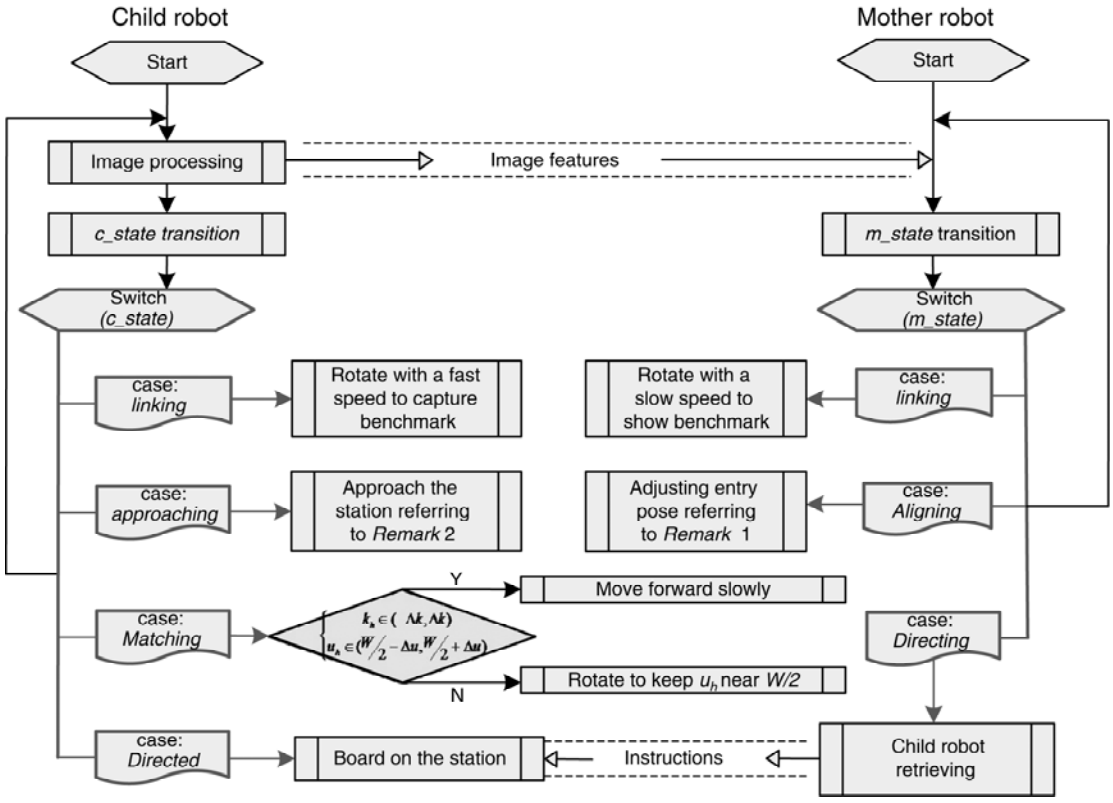

Figure 6. The flow chart of the coordinated docking.

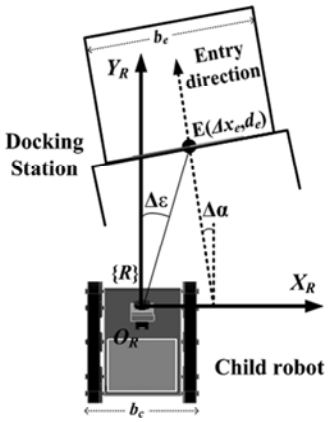

Figure 7. The width deviation and entry direction offset in $\{R\}$.

The influence factors of width deviation Δx_e and entry direction offset $\Delta\alpha$ involve the extracting deviations of image features, the tolerance margins Δu and Δk and the optical deviation angle $\Delta\delta$ of the camera. Among these factors, Δu and Δk are given values and $\Delta\delta$ is available with the specification of the used camera. Therefore, we fix our attention on the extracting deviations of image features. According to the detail depicted in Section 3.1, u_h is the mean horizontal coordinate of pixel points in the chosen candidate group with multiple sub-teams, and every point of which consists of four pixel points surrounding I_h. The centre coordinates of every sub-team are supposed to satisfy a uniform distribution within the range of 8×8 pixels around I_h, and we have the square deviation of centre horizontal coordinate for every sub-team as follows:

$$D_{uf} = \frac{1}{64} \int_0^8 \int_0^8 (u-4)^2 du dv \tag{9}$$

Thus, we estimate the standard deviation E_u of the extracting deviation of u_h with formula:

$$E_u \leq \sqrt{4D_{uf}/T_N} \tag{10}$$

Figure 8 gives the geometry model of field of view (FOV) θ_f and image size for the camera, where W and H are the width and height of image, respectively. Here, we choose the triple standard deviations as the upper limits of the extracting deviations of image features. From Fig. 8, $\Delta\varepsilon$ is deduced as follows:

$$|\Delta\varepsilon| \leq \arctan\left(\frac{3E_u + \Delta u}{\sqrt{H^2+W^2}/2} * \tan(\theta_f/2) + \tan(\Delta\delta)\right) \tag{11}$$

Then, according to $\Delta x_e = d_e \tan(\Delta\varepsilon)$, where d_e is the critical visual perception distance, we have

$$|\Delta x_e| < d_e\left(\frac{3E_u + \Delta u}{\sqrt{H^2+W^2}/2} * \tan(\theta_f/2) + \tan(\Delta\delta)\right) \tag{12}$$

However, as shown in formula (5), the imaging slope k_h shall be calculated by the least square fitting method. Assume that the v-coordinate v_i of every border pixel point

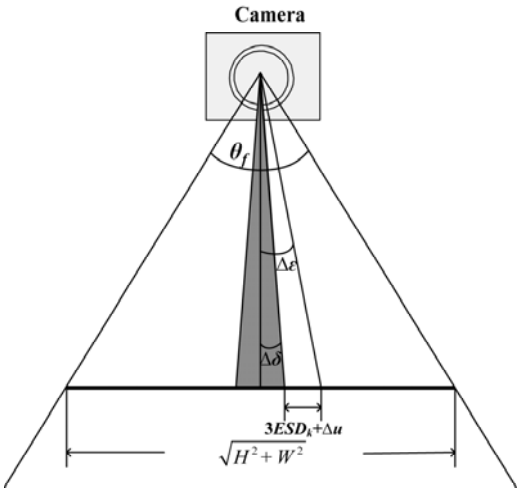

Figure 8. The geometry model of FOV θ_f and image size for the camera.

satisfies a uniform distribution within a range of ± 2 pixels, one can obtain the square deviation of v_i as follows.

$$D_{vi} = \frac{1}{4}\int_{-2}^{2} v^2 dv \tag{13}$$

The standard deviation E_k of the extracting deviation of k_h is calculated as follows:

$$E_k = \sqrt{D\left(\frac{\sum_{i=0}^{s_u}(i-s_u/2)(v_i-\overline{v})}{\sum_{i=0}^{s_u}(i-s_u/2)^2}\right)} \approx \sqrt{\frac{D_{vi}}{\sum_{i=1}^{s_u^e}(i-s_u^e/2)^2}} \tag{14}$$

Combining formulas (6) and (14), we have:

$$\left|\frac{k_y h}{k_x(\Delta x_e + d_e\tan(\Delta\alpha+\pi/2)+h\tan\theta\tan(\Delta\alpha+\pi/2))\cos\theta}\right| < 3\sqrt{\frac{D_{vi}}{\sum_{i=1}^{s_u^e}(i-s_u^e/2)^2}} + \Delta k \tag{15}$$

From formula (15), the upper limit of the absolute value of $\Delta\alpha$ shall be estimated under the condition of $k_x \approx k_y$ as:

$$|\Delta\alpha| < \arctan\frac{d_e + h\tan\theta}{\left|h\sec\theta/(3\sqrt{D_{vi}/\sum_{i=1}^{s_u^e}(i-s_u^e/2)^2}+\Delta k) - |\Delta x_e|\right|} \tag{16}$$

4. Experiments

4.1 The Prototype of Marsupial Robotic System and Precision Calculation

Figure 9 shows the marsupial robotic system prototype used to verify the proposed approach. The related parameters are shown in Table 1.

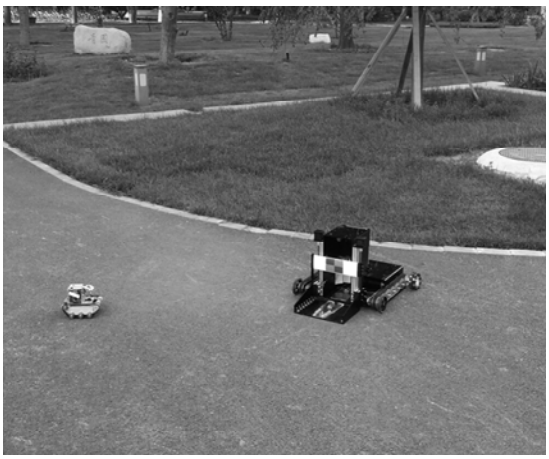

Figure 9. The prototype of experimental marsupial robotic system.

Table 1
Parameters for the Experimental Marsupial Robotic System

Item	Value
Width of entrance of the docking station b_e	19 cm
Width of the child robot b_c	17 cm
Upper obliquity angle of the camera θ	15°
Altitude difference between H_{GS} and the camera h	23 cm
Image size of camera (W × H)	640 × 480
Angle of FOV for the camera θ_f	61°
Optical deviation angle $\Delta\delta$	<1.5°
Threshold used to extract midpoint T_N	32
Image feature tolerance margin Δu	5
Image feature tolerance margin Δk	0.02
Visual perception criterion distance d_e	22 cm
Pre-measured image feature criterion s_u^e	203

Calculate the values of Du_i and Dv_i in formulas (9) and (13), then take them with T_N and s_u^e into formulas (10) and (14), we get $E_u \le 0.8165$ and $E_k \approx 0.0014$. On this basis, we can estimate $|\Delta x_e| < 0.817$ cm and $|\Delta\alpha| < 0.96°$ according to formulas (12) and (16). Then, we have $b_e\cos|\Delta\alpha|/2 > b_e\cos 0.96^\circ/2 = 9.498$ and $|\Delta x_e| + b_c/2 < 0.817 + b_c/2 = 9.317$, which means that the condition for a successful docking represented in formula (8) is satisfied.

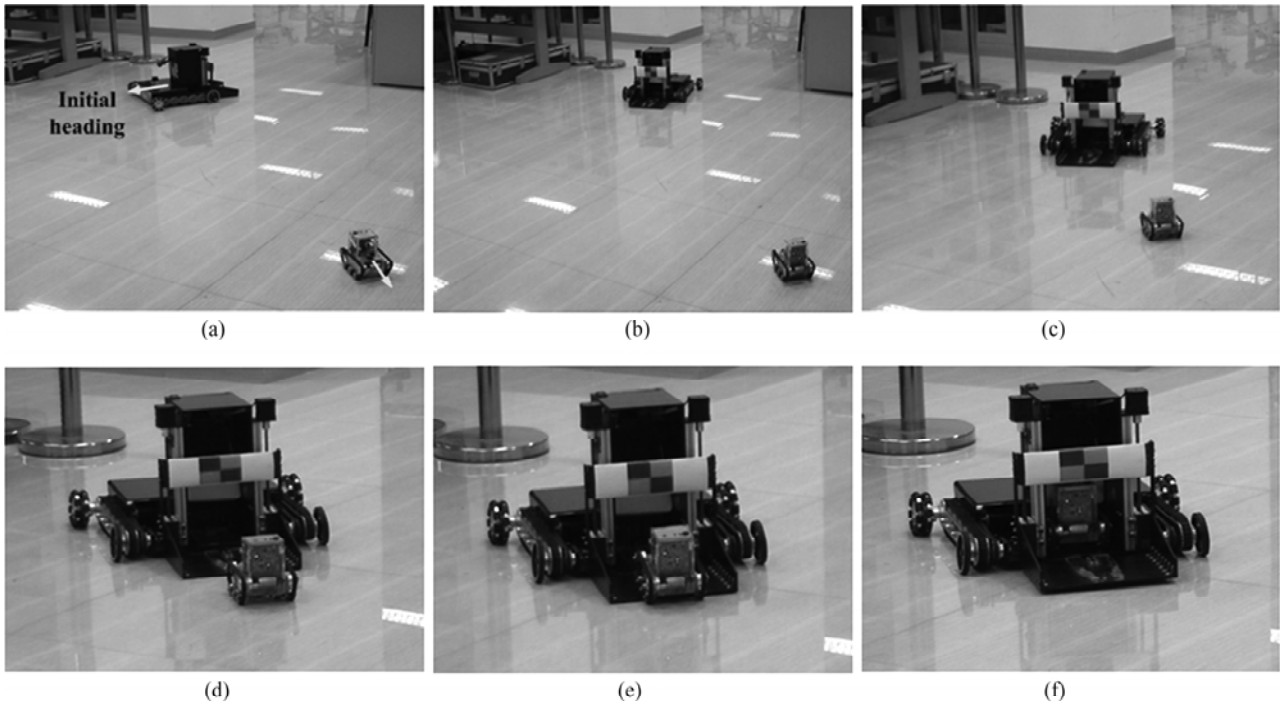

Figure 10. The video snapshots of experiment I.

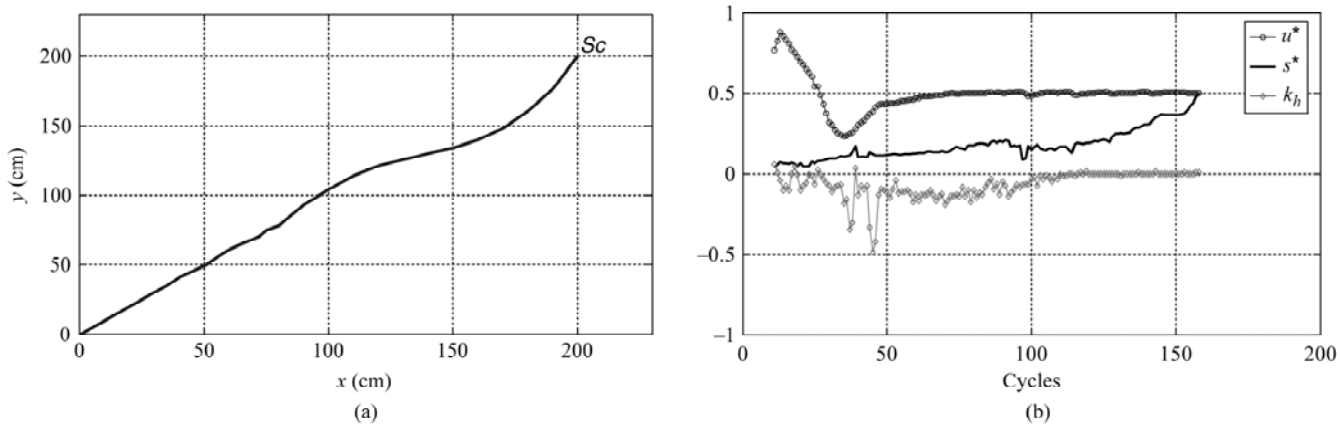

Figure 11. The results of Experiment I: (a) the docking trajectory; (b) the variations of image features.

4.2 The Experimental Results

Several experiments are conducted to test the effectiveness of the proposed coordinated docking approach. Figure 10 gives the video snapshots of experiment I. The docking trajectory of child robot is described in Fig. 11(a), where S_c is the starting position of the child robot with an initial heading back to the mother robot. The variations of image features are depicted in Fig. 11(b), where u^* and s^* are the normalized values of u_h and s_u divided by image width W. One can see that no image features are extracted at the beginning and the two robots are in *linking* state. After the image features are extracted, u^* is adjusted to 0.5 after an overshoot and kept to be near 0.5, which means the benchmark is kept near the centre of the image. The value of s^* increases on the whole trend as the child robot approaches. As to k_h, its value fluctuates obviously at the beginning due to inadequate pixel points for H_{GS} fitting. As s^* increases, k_h becomes sensitive to the motion of the mother robot until it steadies near zero, which manifests that the heading direction of child robot is basically in coincidence with the entry direction of docking station. Finally, the child robot enters the docking station smoothly.

Experiment II considers the case with an interference. Figures 12 and13 show the video snapshots and the result curves, respectively. When the child robot is in position A, it is moved manually to position B with its back towards the benchmark. The variations of task states are depicted in Fig. 14. It can be observed that although the image features are missing, the child robot does not change its *approaching* state immediately but moves a short distance

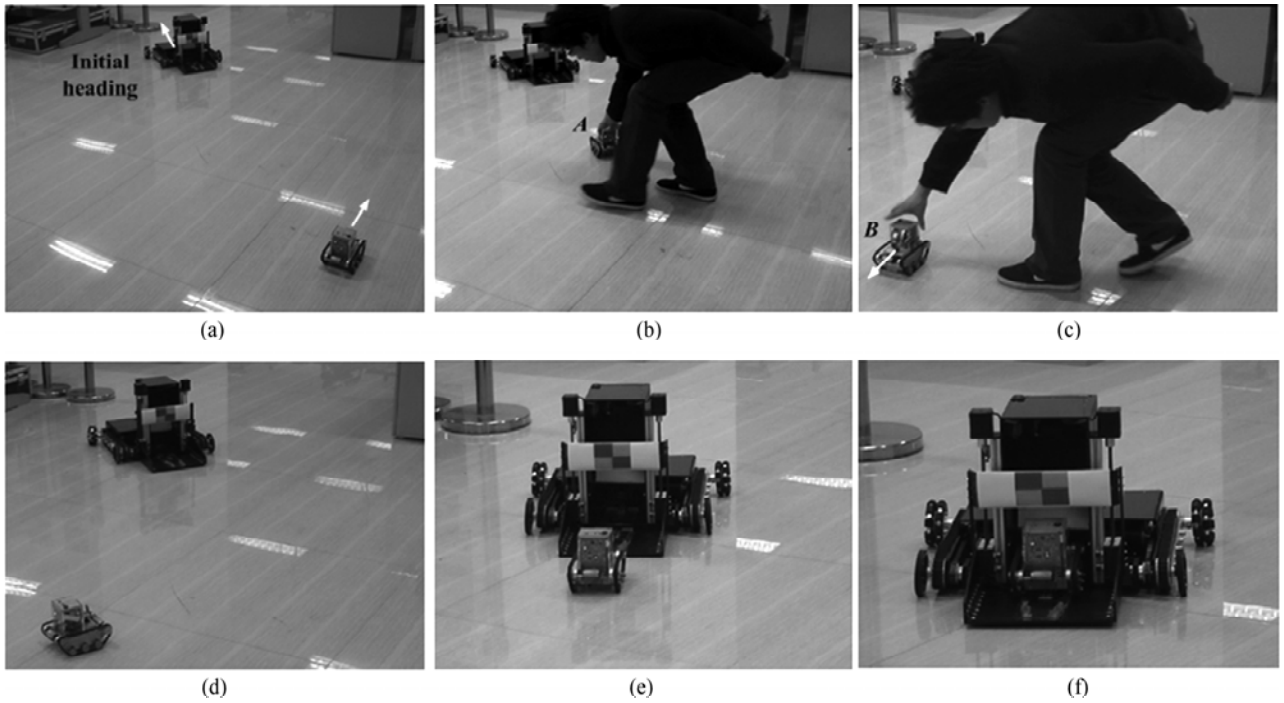

Figure 12. Video snapshots of experiment II.

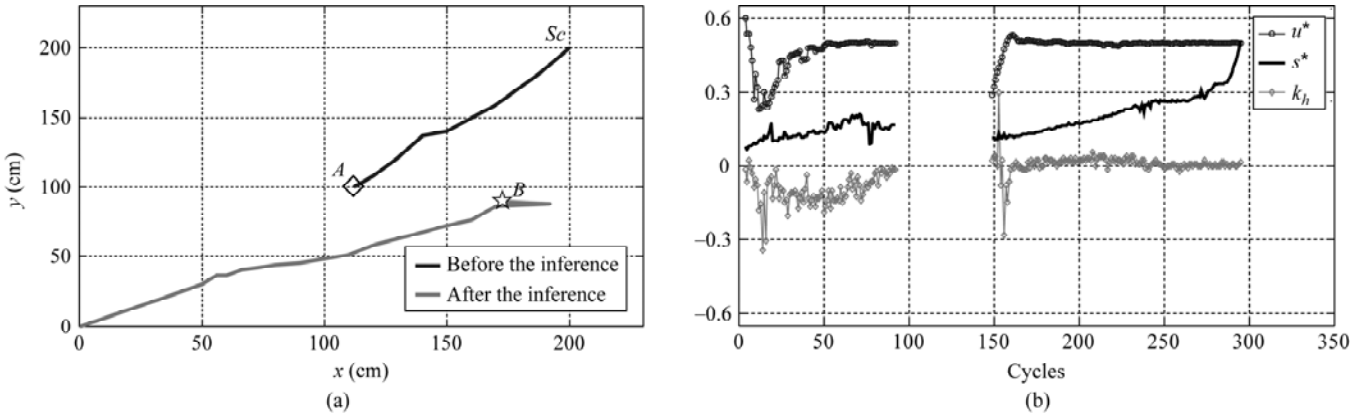

Figure 13. The results of experiment II: (a) the docking trajectory with an interference; (b) the variations of image features.

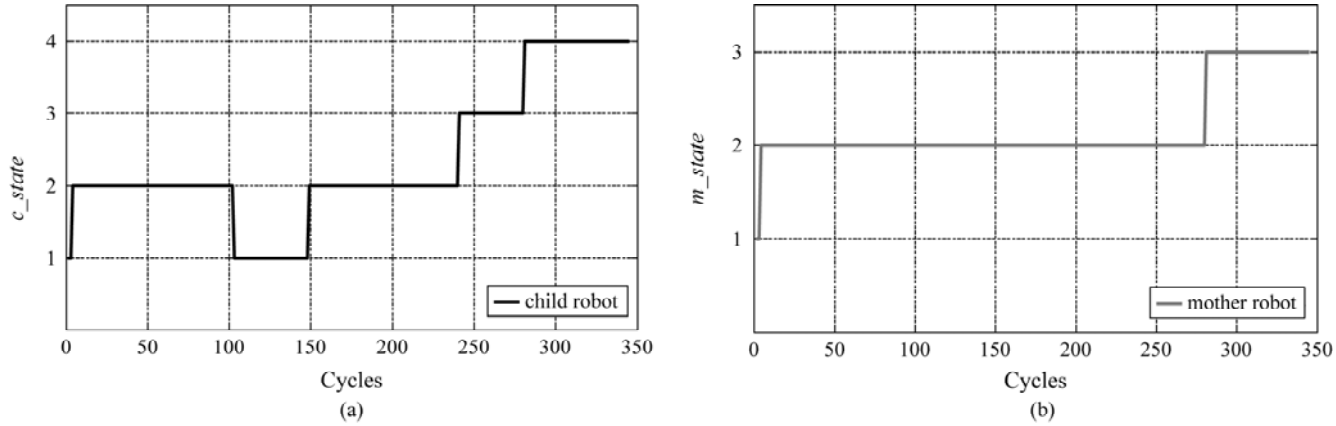

Figure 14. The variations of task states for the child robot and its mother robot. (a) shows the states of the child robot and $c\_state = 1, 2, 3$ and 4 corresponds to *linking*, *approaching*, *matching* and *directed* states, respectively. (b) describes the states of the mother robot and $m\_state = 1, 2$ and 3 corresponds to *linking*, *aligning* and *directed* states, respectively.

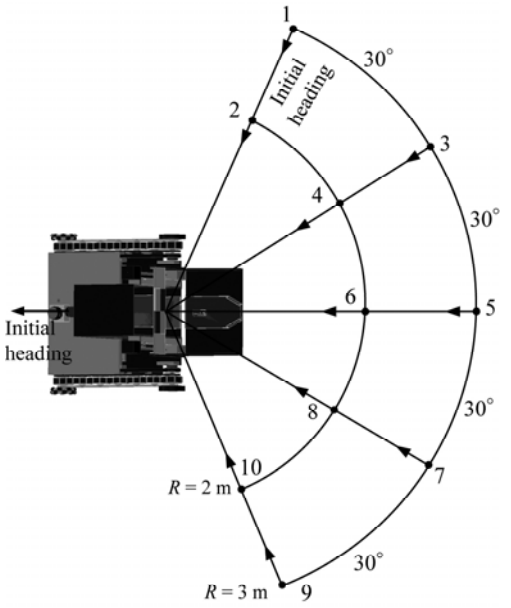

Figure 15. Departure locations of the child robot in experiment III.

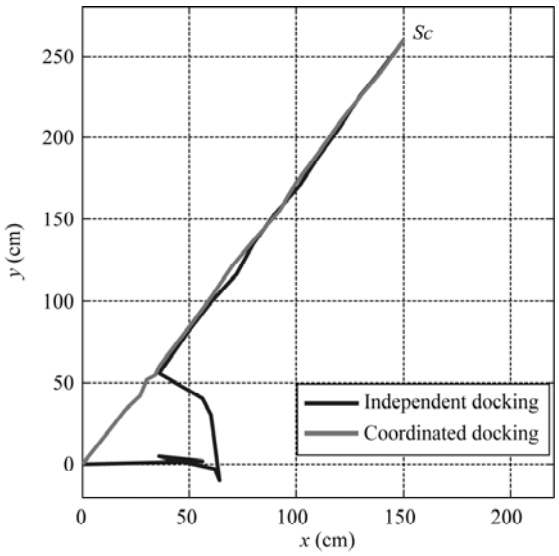

Figure 16. Trajectories of coordinated docking with independent docking in departure location of 1.

until it switches to *linking* state to continue the task, while the mother robot keeps in *aligning* state. Finally, the child robot boards the lifting platform and gets into its storing capsule.

Experiment III describes the comparison in an indoor environment between the coordinated docking approach and the independent docking approach. The latter only considers the autonomous motion of child robot without involving the mother robot. As shown in Fig. 15, 10 departure locations are settled for the child robot. For every location, three trials are executed with each approach. Figure 16 describes the trajectories of these two docking approaches with departure location of 1. It is seen that the trajectory of coordinated docking is evidently shorter than that of the other. Figure 17 gives the comparison of average times with different departure locations for two docking approaches. One can conclude that the coordinated docking is much more economized with most departure locations. As for the locations of 5 and 6, the difference is not obvious because the entry direction of docking station is almost in accordance with the heading of child robot, which means that the mother robot only makes slight adjustment to contribute the coordinated docking.

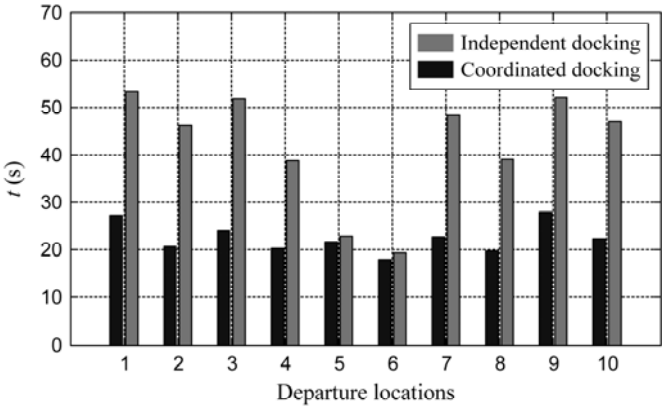

Figure 17. The comparison of average times with different departure locations for two kinds of docking in experiment III.

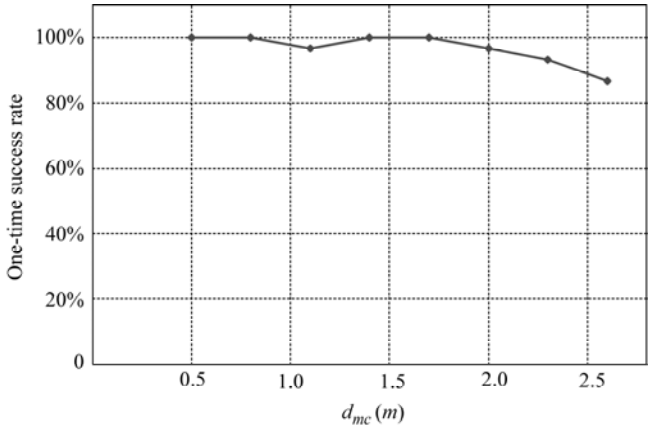

Figure 18. The verification of the repeatability of the proposed approach.

To test the repeatability of the proposed approach, 240 trials are conducted in an outdoor environment as shown in Fig. 9. There are eight grades according to the distance d_{mc} between the mother robot and the child robot, and d_{mc} is chosen from 0.5 m with an increment of 0.3 m. For each grade, 30 trials with random relative directions are executed. The experimental result is shown in Fig. 18, which describes the curve of one-time success rate with the variation of d_{mc}. One can see that the minimal success rate is 86.7% (26 out of 30 trials). A possible reason for a few failure cases comes from a poor image acquisition of CMOS camera utilized by the child robot.

Conclusion

This chapter proposes a coordinated docking approach for a marsupial robotic system with a new docking station to

retrieve/deploy child robots flexibly. Based on the internal correlation between the heading direction of the child robot and the entry direction of docking station, we develop a docking task model, which provides the basis of mother–child coordination. The experiment results show that the proposed approach fulfil a quick docking with a shorter journey and less time consumption It should be noted that the results proposed in this chapter can not only be used for marsupial robotic systems but also contribute to other researches such as the self-reconfigurable robots and intelligent vehicles.

Acknowledgement

This work is supported in part by the National Natural Science Foundation of China under Grants 61273352, 61175111, 61273337, 61305024 and 60805038.

References

[1] A. Bicchi, A. Fagiolini, and L. Pallottino, Towards a society of robots, *IEEE Robotics & Automation Magazine*, *17*(4), 2010, 26–36.

[2] A. Drenner, M. Janssen, A. Kottas, A. Kossett, *et al.*, Coordination and longevity in multi-robot teams involving miniature robots, *Journal of Intelligent and Robotic Systems*, *72*(2), 2013, 263–284.

[3] C.G. Cena, P.F. Cardenas, R.S. Pazmino, L. Puglisia, *et al.*, A cooperative multi-agent robotics system: Design and modelling, *Expert Systems with Applications*, *40*(12), 2013, 4737–4748.

[4] G. Azkune, P. Orduña, X. Laiseca, E. Castillejo, *et al.*, Semantic framework for social robot self-configuration, *Sensors*, *13*(6), 2013, 7004–7020.

[5] J. Oyekan and H. Hu, Biologically-inspired behaviour based robotics for making invisible pollution visible: A survey, *Advanced Robotics*, *28*(5), 2013, 271–288.

[6] H. Pan, X. Nian, and L. Guo, Second-order consensus in multi-agent systems based on second-order neighbours' information, *International Journal of Systems Science*, *45*(5), 2014, 902–914.

[7] R.R. Murphy, M. Ausmus, M. Bugajska, T. Ellis, *et al.*, Marsupial-like mobile robot societies, *Proc. 3rd Intl. Conf. on Autonomous Agents*, Seattle, WA, 1999, 364–365.

[8] M. Lindemuth, R.R. Murphy, E. Steimle, W. Armitage, *et al.*, Sea robot assisted inspection, *IEEE Robotics & Automation Magazine*, *18*(2), 2011, 96–107.

[9] H. Hourani, P. Wolters, E. Hauck, and S. Jeschke, A marsupial relationship in robotics: A survey, *Proc. 4th Intl. Conf. on Intelligent Robotics and Applications*, Aachen, Germany, 2011, 335–345, LNAI 7101.

[10] D. Carroll, H.R. Everett, G. Gilbreath, and K. Mullens, Extending mobile security robots to force protection missions, *AUVSI Unmanned Systems*, Lake Buena Vista, FL, 2002, 9–11.

[11] G.S. Sukhatme, J.F. Montgomery, and R.T. Vaughan, Experiments with cooperative aerial-ground robots, *Robot Teams*, (Natick, MA: AK Peters Ltd, 2002), 345–368.

[12] C. Zhou, Z.Q. Cao, S. Wang, and M. Tan, A marsupial robotic fish team: Design, motion and cooperation, *Science China-Technological Sciences*, *53*(11), 2010, 2896–2904.

[13] M.O. Anderson, M.D. McKay, and B.S. Richardson, Multirobot automated indoor floor characterization team, *IEEE International Conference on Robotics and Automation*, Minneapolis, MN, 1996, 1750–1753.

[14] F. Dellaert, T. Balch, M. Kaess, R. Ravichandran, *et al.*, The Georgia Tech Yellow Jackets: A marsupial team for urban search and rescue, *AAAI Mobile Robot Competition*, Edmonton, Alberta, 2002, 44–49.

[15] R. R. Murphy, Marsupial and shape-shifting robots for urban search and rescue, *IEEE Intelligent Systems and Their Applications*, *15*(2), 2000, 14–19.

[16] J. Zhao, G. Liu, Y.B. Liu, and Y. Zhu, Research on the application of a marsupial robot for coal mine rescue, *Proc. 1st Intl. Conf. on Intelligent Robotics and Applications*, Wuhan, China, 2008, 1127–1136, LNAI 5315.

[17] D.F. Hougen, J.C. Bonney, J.R. Budenske, M. Dvorak, *et al.*, Reconfigurable robots for distributed robotics, *Government Microcircuit Applications Conference*, Anaheim, CA, 2000, 72–75.

[18] C. Carlson, A. Drenner, I. Burt, and N. Papanikolopoulos, Modular mobile docking station design, *Proc. IEEE/RSJ Intl. Conf. on Intelligent Robots and Systems*, Beijing, China, 2006, 4722–4727.

[19] A. Drenner and N. Papanikolopoulos, Docking station relocation for maximizing longevity of distributed robotic teams, *Proc. IEEE Intl. Conf. on Robotics and Automation*, Orlando, FL, 2006, 2436–2441.

[20] A. Kottas, A. Drenner, and N. Papanikolopoulos, Intelligent power management: Promoting power-consciousness in teams of mobile robots, *Proc. IEEE Intl. Conf. on Robotics and Automation*, Kobe, Japan, 2009, 1140–1145.

[21] E. Kadioglu and N. Papanikolopoulos, A method for transporting a team of miniature robots, *Proc. IEEE/RSJ Intl. Conf. on Intelligent Robots and Systems*, Las Vegas, NV, 2003, 2297–2302.

[22] H.J. Min, A. Drenner, and N. Papanikolopoulos, Autonomous docking for an eROSI robot based on a vision system with points clustering, *Proc. Mediterranean Conf. on Control & Automation*, Athens, Greece, 2007.

[23] B W. Minten, R.R. Murphy, J. Hyams, and M. Micire, Low-order-complexity vision-based docking, *IEEE Transactions on Robotics and Automation*, *17*(6), 2001, 922–930.

[24] P. Zhao, Z.Q. Cao, X.C. Chen, and D. Xu, A docking approach for child robot based on vision guiding by mother robot, *Journal of Huazhong University of Science and Technology*, *41*(SI), 2013, 29–431, 435 (in Chinese).

Biographies

Zhao Peng received his B.S. degree in mechanical design and automation science from Beijing Information Science and Technology University, China, in July 2010. He is currently working toward his Ph.D. in control theory and control engineering at the State Key Laboratory of Management and Control for Complex Systems, Institute of Automation, Chinese Academy of Sciences. His research interests include multi-robot system and visual servoing.

Cao Zhiqiang received his B.S. and M.S. degrees from Shandong University of Technology, China, in 1996 and 1999, respectively. In 2002, he received his Ph.D. in control theory and control engineering from Institute of Automation, Chinese Academy of Sciences, Beijing, China. He is currently an associate professor in the State Key Laboratory of Management and Control for Complex Systems, Institute of Automation, Chinese Academy of Sciences. His research interests include multi-robot systems, embedded

vision and visual scene cognition, networked intelligent robotic system, *etc.*

Gu Nong received his B.S. degree from the University of Electronic Science and Technology of China in 1997 and M.S. degree from Beijing Institute of Technology in 2000. In 2003, he received his Ph.D. in control theory and control engineering from Institute of Automation, Chinese Academy of Sciences, Beijing, China. He is currently a research fellow at Centre for Intelligent Systems Research, Deakin University, Australia. His research interests include multi-robot systems and signal processing.

Zhou Chao received his B.S. degree (Hons.) in Automation from Southeast University, Nanjing, China, in July 2003, and his Ph.D. in control theory and control engineering from the Institute of Automation, Chinese Academy of Sciences, Beijing, China, in 2008. Since July 2008, he has been an Assistant Professor in the Key Laboratory of Complex Systems and Intelligent Science, Institute of Automation, Chinese Academy of Sciences, where he has been an associate professor since October 2011. His current research interests include the motion control of robot, the bio-inspired robotic fish and embedded system of robot.

Xu De received his B.S. and M.S degrees from Shandong University of Technology, Jinan, China, in 1985 and 1990, respectively, and his Ph.D. from Zhejiang University, Hangzhou, China, in 2001, all in control science and engineering. Since 2001, he has been with the Institute of Automation, Chinese Academy of Sciences, Beijing, China, where he is currently a professor in the Research Center of Precision Sensing and Control. His research interests include robotics and automation, in particular, the control of robots, such as visual control and intelligent control.

Tan Min received his B.S. degrees from Tsinghua University, Beijing, China, in 1986 and his Ph.D. from Automation, Chinese Academy of Sciences, Chinese Academy of Sciences (IACAS), Beijing, China, in 1990, both in in control theory and control engineering. He is currently a professor in the State Key Laboratory of Complex Systems and Intelligent Science, IACAS. He has published more than 100 papers in journals, books and conference proceedings. His research interests include robotics and intelligent control system.